Atmos. Chem. Phys. Discuss., 10, 23345–23380, 2010
www.atmos-chem-phys-discuss.net/10/23345/2010/
doi:10.5194/acpd-10-23345-2010

Atmospheric Chemistry and Physics Discussions

A upper limit for water dimer absorption in the 750 nm spectral region and a revised water line list

A. J. L. Shillings[1], **S. M. Ball**[2], **M. J. Barber**[3], **J. Tennyson**[3], **and R. L. Jones**[1]

[1]Department of Chemistry, University of Cambridge, Cambridge, CB2 1EW, UK
[2]Department of Chemistry, University of Leicester, Leicester, LE1 7RH, UK
[3]Department of Physics and Astronomy, University College London, London WC1E 6BT, UK

Received: 2 August 2010 – Accepted: 19 September 2010 – Published: 11 October 2010

Correspondence to: R. L. Jones (rlj1001@cam.ac.uk)

Published by Copernicus Publications on behalf of the European Geosciences Union.

Abstract

The absorption of solar radiation by water dimer molecules in the Earth's atmosphere can potentially act as a positive feedback effect for climate change. There seems little doubt from the results of previous laboratory and theoretical studies that significant concentrations of the water dimer should be present in the atmosphere, yet attempts to detect water dimer absorption signatures in atmospheric field studies have so far yielded inconclusive results. Here we report spectral measurements in the near-infrared in the expected region of the third overtone of the water dimer hydrogen-bonded OH_b stretching vibration around 750 nm. The results were obtained using broadband cavity ring-down spectroscopy (BBCRDS), a methodology that allows absorption measurements to be made under controlled laboratory conditions but over absorption path lengths representative of atmospheric conditions. In order to account correctly and completely for overlapping absorption of monomer molecules in the same spectral region, we have also constructed a new list of spectral data (UCL08) for the water monomer in the 750–20 000 cm^{-1} (13 µm–500 nm) range.

Our results show that the additional lines included in the UCL08 spectral database provide a substantially improved representation of the measured water monomer absorption in the 750 nm region, particularly at wavelengths dominated by weak monomer absorption features. No absorption features which could not be attributed to the water monomer were detected in the BBCRDS experiments up to water mixing ratios more than an order of magnitude greater than those in the ambient atmosphere. The absence of detectable water dimer features leads us to conclude that, in the absence of significant errors in calculated dimer oscillator strengths or monomer/dimer equilibrium constants, the widths of water dimer features present around 750 nm must be substantially greater (~100 cm^{-1} HWHM) than those reported at longer wavelengths.

ACPD
10, 23345–23380, 2010

1 Introduction

The absorption of solar radiation by water dimers in the Earth's atmosphere has potentially important consequences for the planet's radiative balance and for amplifying the feedback effects of climate change (e.g., Chýlek and Geldart, 1997). Much of the early laboratory work investigating the spectroscopy of water dimers was performed under the non-equilibrium conditions of molecular beams (Odutola and Dyke, 1980; Huisken et al., 1996; Paul et al., 1997, 1998; Nizkorodov et al., 2005) or, more recently, on dimers formed at very low temperatures inside rare gas matrixes (Bouteiller and Perchard, 2004) and helium nano-droplets (Kuyanov-Prozument et al., 2010). Although offering many insights into the fundamental properties of water dimers (e.g., Fellers et al., 1999), such methods cannot provide direct measurements of water dimer absorptions under "normal" atmospheric conditions (ambient temperatures and pressures, and for typical water monomer amounts). Instead, there have been several attempts to detect signs of water dimer absorption directly in atmospheric field studies, with authors variously reporting a dimer absorption band around 750 nm (Pfeilsticker et al., 2003), a potential weak but inconclusive dimer signal in the same region (Sierk et al., 2004) or no observable dimer absorptions at all (Daniel et al., 1999; Hill and Jones, 2000). The disparity in field results has prompted further laboratory investigations into the absorption properties of the water dimer and/or water continuum under atmospherically relevant conditions. These studies tend to have concentrated on infrared frequencies around the fundamental, first overtone and combination band vibrations of the water monomer. In these regions, absorption features consistent with those expected for the water dimer have been observed underlying the monomer bands (e.g., Ptashnik et al., 2004; Paynter et al., 2007, 2009; Ptashnik, 2008) at frequencies that are broadly consistent with theoretical predictions of the dimer's spectrum (Low and Kjaergaard, 1999; Schofield and Kjaergaard, 2003; Schofield et al., 2007; Garden et al., 2008). Additional laboratory studies at frequencies in between water monomer lines report results that are broadly consistent with models of the water continuum absorption (Aldener et al.,

ACPD
10, 23345–23380, 2010

2005; Cormier et al., 2005). But at higher frequencies, Kassi et al. (2005) were unable to reproduce the 750 nm dimer absorption feature seen in the Pfeilsticker et al. (2003) field observations under analogous conditions in their laboratory.

Here we report results of a broadband cavity ringdown spectroscopy study performed to attempt to detect the third overtone of water dimer's hydrogen-bonded OH_b stretching vibration which the theoretical studies predict to occur around 750 nm with an oscillator strength similar to the monomer itself. As noted previously by Kassi et al. (2005), one very important aspect of spectroscopic studies of the water dimer is the need to account correctly and completely for overlapping absorption of monomer molecules in the same spectral region. For this purpose, and particularly because we probe spectra above room temperature where standard databases can be expected to be less reliable, we have also constructed and tested a new list of spectral data for the water monomer which is reported below.

1.1 Water dimer abundance

Water dimers form in the atmosphere from the (reversible) association of two water molecules. Thus the concentration of water dimers depends on the square of the water monomer concentration via the equilibrium:

$$H_2O + H_2O + M \rightleftharpoons (H_2O)_2 + M \quad (1a)$$

where M is a third body molecule. The water dimer concentration can be found from a rearrangement of the expression for the equilibrium constant for dimer formation:

$$K_{eq} = [(H_2O)_2]/[H_2O]^2 \qquad \text{i.e. } [(H_2O)_2] = K_{eq}[H_2O]^2 \quad (1b)$$

Dimer concentrations in the atmosphere will vary with temperature due to a combination of the equilibrium constant's dependence on temperature, and because the water monomer's saturated vapour pressure increases approximately exponentially with temperature. The literature contains a number of estimates of the equilibrium constant for dimer formation derived from both experimental and theoretical approaches. Curtiss et al. (1979) measured the thermal conductivity of steam over a range of

ACPD
10, 23345–23380, 2010

temperatures and pressures, and then inferred K_{eq} and ΔH (and so too ΔS) for the dimer formation process. Harvey and Lemmon (2004) inferred K_{eq} from second virial coefficient (B) data derived from vaporisation measurements using the relationship $K_{eq}(T) = -(B - b_0)/RT$ where b_0 is the excluded volume. Paynter et al. (2007) estimated K_{eq} by fitting water dimer absorption features (using the theoretical result of Schofield and Kjaergaard, 2003) to residuals remaining after fitting the monomer absorption in water vapour spectra around 3700 cm^{-1}.

The equilibrium constant can also be calculated from the molecular partition functions for the monomer and dimer and the dimer's dissociation energy. The calculation relies on an accurate potential surface being available from which the dimer's energy levels and hence partition function are found (Vigasin, 2000). This theoretical approach is made complicated because some uncertainty exists as to which states should be included when calculating the dimer partition function, in part because the dissociation energy is not sufficiently well constrained. For example, Scribano et al. (2006) showed that an error of 4% (50 cm^{-1}) in the dissociation energy (1234 cm^{-1}, 15 kJ mol^{-1}) could lead to an error of 26 % in the calculated dimer equilibrium constant.

Estimates of K_{eq} from the experimental studies described above and from the theoretical studies of Munoz-Caro and Nino (1997), Goldman et al. (2004) and a further refinement using fewer approximations by the latter group (Scribano et al., 2006) are summarised in the upper panel of Fig. 1. The points represent K_{eq} values reported in the literature, the solid line comes from the study of Scribano et al. (2006) which explicitly addresses the temperature dependence of K_{eq}, and the broken lines were calculated using data given by their original authors assuming that ΔH and ΔS for dimer formation are independent of temperature (an assumption that Scribano et al. (2006) showed is not strictly valid). The main feature of the plot is that K_{eq} decreases rapidly as temperature increases, which is characteristic of a weakly bound molecular complex. There are also significant differences in the various K_{eq} determinations, particularly for the lower temperatures shown on the graph which correspond to those encountered in the atmosphere.

ACPD
10, 23345–23380, 2010

Using the median K_{eq} estimate from Curtiss et al. (1979) for a typical mid-latitude atmospheric temperature (25 °C) and water vapour concentration (4×10^{17} molecule cm^{-3}≈1.6% mixing ratio), the calculated water dimer concentration is 2.4×10^{14} molecule cm^{-3} i.e. 0.06% of the monomer concentration. This low value partly explains why there have been relatively few studies of water dimer absorption under atmospheric conditions and instead water dimers have often been studied using the non-equilibrium conditions of molecular beams where conditions can be adjusted to maximise the mole fraction of the dimer present.

The shaded area of the lower panel of Fig. 1 shows the range of predicted water dimer concentrations as a function of temperature (assuming a relative humidity of 85%, i.e. conditions readily achievable in a laboratory study) for the range of K_{eq} determiations in the figure's upper panel. Although K_{eq} decreases with increasing temperature, dimer concentrations increase rapidly at higher temperatures due to the $[H_2O]^2$ term in Eq. (1b). This also implies that the climate feedback effect of water dimer absorption is likely to be positive.

1.2 Theoretical studies of the water dimer absorption

The vibrational modes of the donor unit of the water dimer are labelled by $|x\rangle_f|y\rangle_b|z\rangle$ where x is the number of vibrational quanta in the unbound "free" OH_f mode, y the number in the OH_b mode (where the H_b atom forms the hydrogen bond) and z the number of bending quanta (see, for example, Schofield et al., 2003). In the acceptor unit, where the two OH bonds are identical, the notation used is $|xy\rangle_{+-}|z\rangle$, with x, y and z having the same meaning as before. The transition of interest for the current work is $|0\rangle_f|4\rangle_b|0\rangle$, i.e. the transition from the vibrational ground state exciting 4 quanta of energy in the OH_b vibrational mode. Transitions of this type are particularly promising for laboratory detection and field observation of water dimer absorption signatures (e.g., Pfeilsticker et al., 2003; Schofield et al., 2007) as the OH_b bond has been weakened by the act of hydrogen bonding and so transitions exciting this bond

ACPD
10, 23345–23380, 2010

are red-shifted. Indeed, the predicted red-shifting is such that these dimer transitions occur at the edges of or even between the main monomer bands where, because the monomer absorption is much weaker, any dimer transitions ought to be more readily identifiable. Thus the spectral region selected for this work (the shaded area in Fig. 2) was chosen to span the positions of the red-shifted $|0\rangle_f|4\rangle_b|0\rangle$ absorption features predicted from theory. The water dimer bands plotted in the lower panel of Fig. 2 have been selected to illustrate the range of band positions and intensities resulting from the different theoretical approaches (Low and Kjaergaard, 1999; Schofield and Kjaergaard, 2003; Schofield et al., 2007). For comparison, the upper panel of Fig. 2 shows high resolution water monomer cross sections calculated using our new UCL08 line list.

To generate the dimer absorption spectra in Fig. 2 we follow the convention of Schofield and Kjaergaard (2003) who assumed a Lorentzian line shape. We have also assumed a line width of 25 cm^{-1} half width at half maximum (HWHM) which is representative of the various experimentally observed features assigned to the water dimer by previous investigators. The features observed by Ptashnik et al. (2004) around 1880 nm (5300 cm^{-1}) had a HWHM of either 18 cm^{-1} or 28 cm^{-1} depending upon which model of the water vapour continuum absorption was used in the retrievals, and those from Paynter et al. (2007) around 2700 nm (3700 cm^{-1}) also had a HWHM of 28 cm^{-1}. In their theoretical paper, Schofield and Kjaergaard (2003) suggest a HWHM of 20 cm^{-1} for water dimer transitions.

2 Broadband cavity ringdown spectroscopy

Broadband cavity ringdown spectroscopy (BBCRDS) uses light from a pulsed broadband laser to measure the spectrum of weakly absorbing samples contained within a high finesse optical cavity (Ball and Jones, 2003, 2009). A multivariate fit of reference absorption cross sections to structured features in the sample's absorption spectrum using an analysis similar to that developed for differential optical absorption spectroscopy (DOAS) (Platt, 1999) is then performed to identify the species that make

ACPD
10, 23345–23380, 2010

structured contributions to the total measured absorption. There are significant advantages of the current BBCRDS approach over that of DOAS. Firstly, since it is possible to record an accurate background spectrum (recorded in the absence of absorbing species), an absolute rather than differential absorption spectrum can be obtained. Consequently it is possible to identify and separately quantify not only structured absorbers present in the total measured signal (water monomer) but also relatively unstructured absorbers whose features vary only slowly with wavelength and may extend over a large spectral range (water dimer). Secondly, conventional DOAS requires the use of very long paths to achieve the sensitivity necessary to investigate weak absorptions. Such paths can only be realised in the real atmosphere where experimental conditions (temperature and $[H_2O]$) cannot be controlled and are potentially inhomogeneous over the light path. In BBCRDS, the very long effective pathlengths (up to 60 km in this work) are achieved within an absorption cell, defined by a high finesse cavity that is only some 2 m in length, thus enabling experimental conditions to be tightly and reproducibly controlled.

A broadband dye laser pumped by a 532 nm Nd:YAG laser (Sirah Cobra and Sure-light I-20) generated light pulses (10 ns, 20 Hz repetition rate) with an approximately Gaussian emission spectrum centred at 748 nm (FWHM=16.5 nm). This light was directed into a 196 cm long ringdown cavity formed by two highly reflective mirrors (Los Gatos, measured peak reflectivity=99.994% at 765 nm). Light exiting the ringdown cavity was collected and conveyed through a 200 µm core diameter fibre optic cable to an imaging spectrograph (Chromex 250is) where it was dispersed in wavelength and imaged onto a clocked CCD camera (XCam CCDRem2). The time evolution of individual ringdown events was recorded simultaneously at 512 different wavelengths, one for each pixel row of the detector, and light from 50 ringdown events was integrated on the CCD camera before storing the data to a computer. Wavelength resolved ringdown times were produced by fitting the ringdown decay in each pixel row. The sample's absorption spectrum was then calculated from sets of ringdown times measured when

ACPD
10, 23345–23380, 2010

the cavity contained the sample, $\tau(\lambda)$, and when flushed with dry synthetic air, $\tau_0(\lambda)$:

$$\alpha(\lambda) = \frac{R_L}{c}\left(\frac{1}{\tau(\lambda)} - \frac{1}{\tau_0(\lambda)}\right) = \alpha_{\text{cont}}(\lambda) + \sum_n \alpha_n(\lambda) \quad (2)$$

Here c is the speed of light, R_L is the fraction of the cavity that is occupied by absorbing species, $\alpha_n(\lambda)$ is the wavelength dependent absorption coefficient of the n^{th} molecular absorber and $\alpha_{\text{cont}}(\lambda)$ is any remaining unstructured continuum absorption.

A known complexity that must be accounted for in the analysis of BBCRDS spectra is the apparent non-Beer-Lambert law behaviour exhibited by strong absorption lines that are not fully resolved at the limited resolution of the instrument's spectrograph (here 0.22 nm FWHM). As discussed in detail in Ball and Jones (2003), Bitter et al. (2005) and Ball and Jones (2009), this effect is treated quantitatively using linearised absorption cross sections, and this approach was adopted here from the water monomer.

Measurements were made on continuously flowing gas samples supplied to the ring-down cavity via flow controllers, a temperature regulated water bubbler and particle filters. The temperature inside the cavity was controlled by circulating heated/cooled water from a thermostated water bath through an insulated, double-walled glass vessel running the length of the cavity. Gas delivery lines were constructed to prevent coldspots and passed between the glass vessel and its insulation in order to prevent condensation and to enable the gas supply to be admitted at the same temperature as the cavity itself. Temperatures between 5 and 95 °C and relative humidities up to 95% were achieved with no aerosol formation and negligible temperature gradients along the cavity. The gas flow exited past the cavity mirrors and was vented into the laboratory: thus all experiments were performed under ambient pressure with the sample occupying the whole cavity (R_L=1 in Eq. 2). To prevent condensation of water vapour on the surface of the cavity mirrors (which would have reduced their reflectivity and produced an anomalous absorption signal), the mirrors were held in temperature controlled mirror mounts regulated at approximately 3 °C above the cavity's temperature. This approach was found both to eliminate condensation on the mirror surfaces and,

ACPD
10, 23345–23380, 2010

somewhat unexpectedly, to improve the reflectivity of the mirrors by approximately 10% relative to that at room temperature, presumably due to desorption of adsorbed species from the hot mirror surfaces.

3 The UCL08 line list

The HITRAN 2008 database (Rothman et al., 2009) provides a good quality reference for water's strong absorption lines in most spectral regions. However, having a relatively high cut-off in line strength intensity, it omits many weak lines which are known to be present from ab initio calculations and which can become important in long path length absorption experiments such as those reported here. The present line list, which we name UCL08, therefore attempts to fill in such gaps as there are in the HITRAN database by using a combination of new experimental data (see below) and, in the absence of measurements, theoretical lines from the calculated BT2 linelist (Barber et al., 2006). To improve the accuracy of the calculated transition frequencies, a version of BT2 modified to use experimental energy levels from Tennyson et al. (2001) rather than purely theoretical ones was used. Figure 3 shows a comparison of high resolution water monomer cross sections calculated from the HITRAN08 and UCL08 line lists in the region of the $|0_f|4\rangle_b|0\rangle$ dimer absorption, and illustrates the large number of additional lines at the edge of the water monomer band present in the new line list. Note also that these extra lines tend to increase in intensity at the elevated temperatures used in the BBCRDS experiments, as demonstrated in the lower panel of Fig. 3 which shows a comparison of HITRAN08 and UCL08 monomer cross sections calculated for 368 K.

The UCL08 linelist covers the 750–20 000 cm^{-1} range at the default HITRAN temperature of 296 K and was constructed as follows. Lines were matched between HITRAN and the other sources where possible by rigorous quantum numbers. Lines from new experimental sources (Jenouvrier et al., 2007; Mikhailenko et al., 2007, 2008; Coudert et al., 2008; Tolchenov and Tennyson, 2008) are taken in preference to HITRAN. Where both transitions are present, lines from HITRAN were used in preference to

ACPD
10, 23345–23380, 2010

theoretical data except in the 8000–9500 cm^{-1} spectral region where there is a systematic intensity-weighted average difference of around 20% (see Fig. 4), the HITRAN lines being weaker than those in the UCL08 database. Support for our use of the theoretical intensities from the BT2 linelist as first preference for UCL08 in the 8000–9500 cm^{-1} region is provided by Casanova et al. (2006) who compared high resolution Fourier transform measurements of solar radiation at ground level with that modelled using HITRAN04 water vapour lines: whilst there was good agreement in other spectra regions, the modelled absorption underestimated the measured absorption by 18% between 8000 and 9500 cm^{-1} (a similar difference to that in the cross sections ratios shown in Fig. 4). In other regions, the UCL08 and HITRAN08 average line strengths typically agree to within 2.5% (see also Fig. 4) which is within the uncertainty of the new database. Lines in HITRAN are given the same line width parameters in UCL08. Line widths for non-HITRAN lines were estimated using a method based on fitting to lines with similar quantum numbers (Voronin et al., 2010). This method has been demonstrated to provide a reasonable fit to known widths given in HITRAN.

There are two versions of the new linelist. One contains around two hundred thousand lines with an integrated line intensity cut-off at $S=10^{-30}$ cm molecule^{-1}, whereas the longer version has around 1.5 million lines with a 10^{-36} cm molecule^{-1} cut-off. The short list should be sufficient for comparison with experimental results in most regions. The long list should provide a good model for water vapour spectra up to about 300 °C, and for high temperatures use of BT2 directly is recommended. Both new line lists are presented in the supplementary data for this article, together with a file of temperature-dependent line strengths (296–368 K) for the nearly sixty thousand lines from the short list in the frequency range 12 750–20 000 cm^{-1}.

ACPD
10, 23345–23380, 2010

4 Results

4.1 BBCRDS measurements in the 750 nm spectral region

As noted above, when searching for water dimer absorption signals, it is vital to account fully for water monomer lines in measured spectra, including weak lines at the edge of the monomer's absorption bands some of which may be incorrectly parameterised (or indeed missing) for spectral databases. In order to test the efficacy of our new water line list relative to the HITRAN08 line list (Rothman et al., 2009), BBCRDS spectra of water vapour were recorded in synthetic air for a variety of water vapour concentrations and temperatures in the spectral region expected for the dimer's $|0\rangle_f|4\rangle_b|0\rangle$ overtone. As an example, the top panel of Fig. 5 shows a BBCRDS spectrum of water vapour in air obtained at 312 K with a water concentration of 1.41×10^{18} molecule cm^{-3} (≈85% relative humidity at 312 K). The elevated temperature is used here i) to increase the water monomer concentration above that at room temperature in order to also increase the intensity of weak water monomer lines and ii) to test the water databases under the experimental conditions that will be used to maximise the water dimer number density in the gas sample during experiments targeting the dimer (cf. the discussion in Sect. 1.1). The red line overlaying the blue BBCRDS spectrum is the fitted water monomer absorption calculated using linearised absorption cross sections at the BBCRDS spectrometer's resolution, constructed using the HITRAN08 line list. The HITRAN spectrum accounts reasonably well for the water monomer lines, yet small systematic differences remain in the residual spectrum (measured minus fitted; black line). The middle panel of Fig. 5 shows the same BBCRDS spectrum (blue), but this time fitted with linearised absorption cross sections calculated using the UCL08 line list (red). Some small features again remain in the residual spectrum (black).

The bottom panel of Fig. 5 shows the residuals from the upper two panels plotted on an expanded vertical scale. Although neither spectral database provides a comprehensive description of the water monomer lines, the standard deviation of the UCL08 residual (5.31×10^{-9} cm^{-1}) is somewhat smaller than for HITRAN08 (5.75×10^{-9} cm^{-1}).

ACPD
10, 23345–23380, 2010

The UCL08 line list generally provides a better fit to the strong water lines on the edge the monomer band at short wavelength; it also has smaller residuals at wavelengths longer than 745 nm where, there being only weak monomer absorption, the residual is mainly due to measurement noise. In contrast, the HITRAN08 residual shows a broad positive feature in the region 745–752 nm, similar in some respects to a dimer absorption feature. However we discount this as a possible dimer feature because it scales approximately linearly (rather than quadratically) with water monomer concentration and because it is not reproduced using the UCL08 line list that provides the better fit to the water monomer lines in this spectral region. Instead this feature is probably a consequence of weak monomer lines missing from HITRAN08 but included in the UCL08 list, and similar effects have been noted in this region when using other water line lists to fit the water monomer absorption (Kassi et al., 2005). In contrast, no dimer-like absorption features are immediately obvious in the UCL08 residual.

4.2 Comparison with dimer absorption features

BBCRDS measurements of water vapour absorption under conditions similar to those used by Pfeilsticker et al. (2003) were made to attempt to reproduce the absorption feature attributed by these authors to the water dimer. The feature measured by Pfeilsticker et al. (2003) is described by a Lorentzian profile centred at 749.5 nm (13 342 cm^{-1}) with a FWHM of 19.4 cm^{-1} and a peak absorption of 2.5×10^{-9} cm^{-1}. The path averaged temperature and water vapour concentration for their measurement were 292.4 K and 3.6×10^{17} molecule cm^{-3}.

The new UCL08 water database, which was shown in the previous section to provide the best representation of water monomer absorption in this spectral region, was exclusively used for the analysis of the BBCRDS spectra presented in this and following sections. Panel 1A of Fig. 6 shows a BBCRDS absorption spectrum (blue) recorded at a water concentration of 3.97×10^{17} molecule cm^{-3} and a temperature of 297 K, conditions that are similar to those of the Pfeilsticker et al. (2003) measurement in the ambient atmosphere. The red spectrum is the fitted water monomer signal and the

ACPD
10, 23345–23380, 2010

black line is the residual remaining in the BBCRDS spectrum after subtraction of the fitted monomer absorption. Panel 1B of the same figure shows the residual re-plotted on a larger scale (black), together with a Lorentzian function representing the Pfeilsticker et al. (2003) absorption feature (PAF) that has been scaled to account for small differences between the Pfeilsticker et al. (2003) conditions and those of the BBCRDS measurement. Here the PAF has been assumed to scale with the square of the water monomer concentration and scale according to the temperature dependence of the Curtiss et al. (1979) $K_{eq}(T)$ data. It is evident that, at this water concentration, the measurement residuals are of the same magnitude as the Pfeilsticker et al. (2003) feature, and no unequivocal conclusions can be drawn. However, as indicated above, we are able with the BBCRDS measurements to increase the water monomer concentrations, and hence too the dimer amount, by performing experiments at elevated temperatures.

Panel 2A of Fig. 6 shows the measured (blue), fitted (red) and residual (black) spectra recorded for a water concentration of 5.0×10^{17} molecule cm^{-3} at a temperature of 312 K. Panel 2B shows the residual spectrum together with the PAF scaled for the conditions of the BBCRDS measurement. Note that the PAF scaled to these conditions is almost the same size as that in Fig. 1B, the slightly greater water monomer concentration offset by the reduction in K_{eq} at this higher temperature. Once again there is no clear sign of the PAF in the BBCRDS residual. Panels 3A and 3B were also obtained at 312 K but now with water number densities around three times larger (1.4×10^{18} molecule cm^{-3}) than in previous panels. Allowing for the increased number density of water molecules and for the temperature dependent equilibrium constant (but not any changes in dimer line strength) would predict a PAF approximately a factor of ten larger than in the previous panels (hence also a factor of ten larger than for the conditions prevailing in the Pfeilsticker et al. (2003) study). Visual inspection indicates little sign of a PAF signal: the peak-to-peak and RMS of the Panel 3B residual spectrum are, respectively 5.1×10^{-9} and 1.3×10^{-9} cm^{-1}, i.e. ×5 and ×21 smaller than the scaled PAF for these conditions (peak intensity=2.7×10^{-8} cm^{-1}). The conclusion is that either the PAF is not due to water dimer, or the variation of K_{eq} with temperature is

ACPD
10, 23345–23380, 2010

incorrect. However, even using the lowest estimate of K_{eq} from Munoz-Caro and Nino (1997) (which is approximately 33% of the Curtiss et al. (1979) value) would lead to a clearly observable PAF signal in the BBCRDS residual in Panel 3B.

The conclusion, therefore, is that the assignment of the PAF to water dimer absorption is erroneous, a conclusion also later reached by the original authors (Lotter, 2006; personal communication from K. Pfeilsticker cited by Garden et al., 2008). The water monomer line list used by Pfeilsticker et al. (2003) to fit their observed spectra became HITRAN04. In their high resolution cavity ringdown study, Kassi et al. (2005) identified and assigned some 200 additional water monomer lines beyond those included in HITRAN04 in the spectral region of the Pfeilsticker et al. (2003) measurements. The integrated intensity of these additional lines comprised the majority fraction of the PAF's intensity, leading Kassi et al. (2005) to question Pfeilsticker et al.'s (2003) interpretation that they had identified a dimer absorption signal. Since the Kassi et al. (2005) work, HITRAN has been substantially updated around 750 nm using the experimental data of Tolchenov and Tennyson (2008). Yet in ongoing parallels with Kassi et al. (2005), we noted in the previous section that fitting BBCRDS spectra with water monomer cross sections calculated from HITRAN08 could also produce a broad weak feature in the residual around 745–752 nm (bottom panel of Fig. 5). As demonstrated again in this section, no such feature is apparent when using the UCL08 line list, and neither have we found evidence for a PAF with UCL08.

4.3 Characterisation of an upper limit on the water dimer absorption

The fact that no absorption features that can unambiguously be assigned to water dimer absorption have been found in the residuals of water vapour spectra reported in this work implies that one or more of the assumptions used to estimate the dimer absorption must be incorrect (the water dimer abundance i.e. $K_{eq}(T)$; the dimer's calculated line strength; the position and shape of the dimer absorption features). In an attempt to constrain this further, we determine upper limits for water dimer absorption in the present 736–759 nm spectral region by considering what signal, if any, remains

ACPD
10, 23345–23380, 2010

in the residual spectrum of a BBCRDS measurement that cannot be attributed to water monomer absorption using the UCL08 database. The BBCRDS measurement at $[H_2O]=1.41\times10^{18}$ molecule cm^{-3} and 312 K was selected for this analysis (Panel 3B of Fig. 6), since these conditions are expected to produce the greatest dimer absorption signal. The fitted BBCRDS spectrum's residual, shown again on an expanded scale in Fig. 7, contains some systematic structure much of which is undoubtedly the result of still imperfect treatment of the water monomer absorption but which, nevertheless, could overly a weak dimer signal.

To derive upper limits for possible water dimer absorption, the approach taken was to fit Lorentzian functions with variable widths, representative of water dimer absorption features of differing widths, to the BBCRDS residual. Fig. 7 shows fitted Lorentzian features constrained to be centred at 13 495 cm^{-1} (741.0 nm), i.e. at the Hartree–Fock prediction of Low and Kjaergaard (1999), with example HWHMs of γ=2, 20 and 100 cm^{-1}. There happens to be a positive feature in the BBCRDS residual spectrum at 13 495 cm^{-1} which, for the narrowest dimer line width considered here, leads the Lorentzian line fitting routine to produce a putative dimer absorption signal peaking around 1×10^{-8} cm^{-1}. However, the peak of this fitted Lorentzian quickly reduces as the line width broadens to more realistic values for a dimer absorption band as more negative (and only weakly positive) residual structure becomes incorporated into the fit.

The black dots shown in Panel A of Fig. 8 represent the peak intensity of the Lorentzian function (centred at 13 495 cm^{-1}) that can be fitted to the BBCRDS residual spectrum plotted against the Lorentzian's HWHM width. The pink region shows the 1σ uncertainty in the fitted Lorentzian's intensity. The various lines in the blue region show the expected peak absorption for a Lorentzian shaped dimer feature calculated for different literature values of K_{eq} (same as the legend to Fig. 1) and half-widths (γ) using Eq. (3):

$$\text{Peak absorption} = \frac{S\times[H_2O]^2\times K_{eq}}{\pi\times\gamma} \quad (3)$$

ACPD
10, 23345–23380, 2010

where, for Panel A, the dimer line strength was assumed to be the Hartree–Fock value of $S=4.83\times10^{-22}$ cm molecule^{-1} from Low and Kjaergaard. The lower and upper boundaries of the blue region thus correspond to the minimum/maximum K_{eq} estimates of Munoz-Caro and Nino (1997) and Goldman et al. (2004), respectively.

Taking the K_{eq} estimate of Curtiss et al. (1979) as i) intermediate and hence representative of all the available K_{eq} values, and ii) a K_{eq} determined from experiment, the plot in the upper panel of Fig. 8 indicates that the HWHM of any water dimer feature must be rather larger than 100 cm^{-1} because at no point on the graph does the upper limit for dimer absorption from fitting the BBCRDS residual (top of of pink region) coincide with the theoretical prediction of water dimer absorption (Curtiss K_{eq}=thick black dashed line in the blue region). If however one assumes that the lowest K_{eq} estimate of Munoz-Caro and Nino (1997) is correct, then the measurements imply a minimum HWHM consistent with the upper limit on our experimental uncertainty of approximately 20 cm^{-1} (or more likely 30 cm^{-1} HWHM for the optimum Lorentzian fit, black points). Thus the analysis here leads to a HWHM-dependent upper limit for the water dimer absorption signal, dependent also on which K_{eq} is adopted. It should be noted that the discussion assumes that the chosen theoretical prediction of the water dimer line parameters is correct. (Low and Kjaergaard (1999) produced another prediction of this dimer band's position and line strength using a quadratic configuration interaction level of theory: 13 403 cm^{-1} (746.1 nm) and 3.04×10^{-22} cm molecule^{-1}. These values happen to be close to those considered in the next paragraph, where we would expect the same conclusions to apply.)

Panel B of Fig. 8 has the same format as Panel A except that the central wavelength of the fitted Lorentzian function and the water dimer line strength are now constrained at 13 401 cm^{-1} (746.2 nm) and 2.83×10^{-22} cm molecule^{-1}, respectively (Schofield and Kjaergaard, 2003). For this case, the peak absorption is negative for narrow Lorentzian features due to negative structure (measurement noise and/or imperfectly fitted water monomer absorption) being present in the residual spectrum at this centre frequency. Again, the main conclusion is that if the K_{eq} values of Curtiss et al. (1979) and Munoz-

ACPD
10, 23345–23380, 2010

Caro and Nino (1997) are adopted, the minimum HWHM for dimer transitions must be greater than 100 cm^{-1} or around 40 cm^{-1} respectively to be consistent with the upper uncertainty limit in any dimer-like Lorentzian feature present in the BBCRDS residual spectrum (top of the pink shaded region) or rather more than 100 cm^{-1} or around 80 cm^{-1}, respectively for the optimum fitted Lorentzian functions (black dots).

Panel C of Fig. 8 assumes the Lorentzian dimer feature lies at 13 208 cm^{-1} (757.1 nm) with a line strength of 5.93×10^{-22} cm molecule^{-1} according to the AVQZ numeric potential energy curve calculation preferred by Schofield et al. (2007). At this wavelength, the inferred minimum HWHM of dimer transitions is greater than 100 cm^{-1}, irrespective of the choice of K_{eq}. Panel C also shows that the peak intensity of the Lorentzian function constrained at 757.1 nm is the smallest of the three cases considered so far because it is furthest removed from the strong monomer lines of the neighbouring water absorption band, occurring instead in a "quiet" region between monomer bands where the least residual structure remains in the fitted BBCRDS spectrum.

Similar conclusions are drawn when the wavelength restriction is lifted and Lorentzian functions of variable HWHM are now fitted sequentially at centres every 2 cm^{-1} between 13 586 and 13 166 cm^{-1}. Here the dimer line strength was taken to be the most restrictive of those from the theoretical calculations ($S=2.83\times10^{-22}$ cm molecule^{-1}; Schofield and Kjaergaard, 2003). The black dots in the upper panel of Fig. 9 now show the mean peak intensity of the many Lorentzian functions fitted over this frequency range, and the pink region denotes one standard deviation about their mean intensity. Again, the minimum HWHM of the dimer absorption must be greater than 100 cm^{-1} to be consistent with the preferred Curtiss et al. (1979) value of K_{eq}. Using the greater line strengths from Low and Kjaergaard (1999) or Schofield et al. (2007) increases the predicted dimer peak absorption even further above the maximum signal remaining in the BBCRDS residual spectrum, again confirming that any dimer feature residing in the BBCRDS residual must be very wide indeed.

Equivalently, via a rearrangement of Eq. (3), one can assume that a particular K_{eq} is correct, and then infer the line strength of a dimer transition that would be necessary

ACPD
10, 23345–23380, 2010

to reproduce the maximum Lorentzian function consistent with the BBCRDS residual – see the lower panel of Fig. 9. The analogous result is obtained: only the smallest K_{eq} values are consistent with the Lorentzian dimer absorptions fitted to the BBCRDS residual spectrum, and only then for HWHM values greater than at least 80 cm^{-1} assuming the weakest of the line strengths predicted by theory (horizontal red line; Schofield and Kjaergaard, 2003). The dimer's Lorentzian halfwidth has to be substantially greater than 100 cm^{-1} for the upper limit of any signal in the BBCRDS residual to be consistent with the line strengths predicted by Low and Kjaergaard (1999) or Schofield et al. (2007) (blue or black lines), particularly if the Curtiss et al. (1979) equilibrium constant is adopted.

5 Discussion of results

From the water vapour dimer perspective, the main conclusion of the work presented here is that the line shape of any water dimer absorption in the present 750 nm region must be rather wider than those previously observed for smaller excitations at frequencies further into the infrared (Ptashnik et al., 2004; Paynter et al., 2007; Ptashnik, 2008). The minimum HWHM for dimer transitions inferred here depends on both the value of K_{eq} and the dimer line strength calculated by theory, and hence an error in either (or both) of these quantities would impact our conclusion. If the smallest K_{eq} values are used, then relatively narrow (HWHM≈25 cm^{-1}) water dimer features could be consistent with the residuals in our BBCRDS spectra. But it has become generally accepted (Ptashnik, 2008) that K_{eq} is uncertain by no more than approximately ±25% about the Curtiss et al. (1979) data, and thus the upper limits placed on the dimer absorption from this work are more likely only consistent with a very broad dimer absorption (HWHM>100 cm^{-1}). This assumes that the dimer line strength calculated by theory is broadly correct, and indeed the line strengths are generally thought to be uncertain by only a factor of two. For example, the range of intensities predicted by the

ACPD
10, 23345–23380, 2010

many different levels of theory considered by Schofield et al. (2007) spans a factor of two. A similar conclusion can be drawn from the intensities of the various calculated dimer spectra shown in the bottom panel of Fig. 2 which were deliberately chosen to span the full range of band positions and band intensities represented in recent literature. Temperature effects, other than for the monomer concentration and equilibrium constant which are already considered, are not expected to change our main conclusion because variation in the dimer line strength with temperature is thought to be small (around 10% over the temperature range of this study) (Paynter, 2008).

After the reported water dimer detection by Pfeilsticker et al. (2003), Suhm (2004) commented that one would expect the overtone transitions of a relatively weakly bound species such as the water dimer to be considerably broader (by up to an order of magnitude) than the 9.7 cm^{-1} HMHM inferred by Pfeilsticker et al. (2003) because, at ambient temperature, the lifetime of an individual dimer is sufficiently short that a range of hydrogen bond strengths are likely within a collection of dimer molecules. A further effect and one that until recently was not included in theoretical calculations is the coupling with other intra-molecular oscillations which can lead to a considerable broadening of spectral structure. The theoretical study of Garden et al. (2008) attempted to include these coupling effects when calculating the band profiles for water dimer transitions. Although Garden et al. (2008) still only considered transitions between a restricted number of dimer vibrational states, their calculations did address the most important O-O stretching motion, excitation of which has the greatest effect in modifying the potential energy curve for the hydrogen-bonded OH stretch. Garden et al.'s (2008) results suggest that, whilst each transition may only be around 20 cm^{-1} HWHM, the summation of many vibrational bands is likely to produce a much broader feature (in the limit, something more like a continuum), with the intensity of a given OH_b stretching overtone now shared between many simultaneously excited O–O stretches. Garden et al. (2008) also found that the effective widths of transitions increased with increasing overtone, with the HWHM of the dimer features around 5300 cm^{-1} being in good agreement with the observations by Ptashnik et al. (2004)(although there were

ACPD
10, 23345–23380, 2010

discrepancies in the calculated band intensity attributed by Garden et al. (2008) to their simplistic treatment of the OH_b and OH_f stretching modes as uncoupled Morse oscillators). In the near-IR region investigated in the present work, the superposition of multiple OH_b water dimer transitions simultaneously promoting different excitations elsewhere in the dimer molecule was calculated to be very broad, covering several hundred cm^{-1} (so HWHM of the order of at least $100\,cm^{-1}$), and as such is entirely consistent with our own conclusion.

Our results may also explain why previous attempts to search for signs of water dimer absorption in the atmosphere itself have been unsuccessful or inconclusive (e.g., Daniel et al., 1999; Hill and Jones, 2000; Sierk et al., 2004). It was not because the calculated dimer line strength was incorrect, as was supposed at the time, but because the width of the transitions are probably so large that any dimer signals that may have been present in the measured spectra would easily have been lost in the experimental noise and/or removed as the fitted broadband continuum in any DOAS analysis.

6 Conclusions

The intention of this work was to search for signs of water dimer absorption at wavelengths around 750 nm where theoretical studies predict the $|0\rangle_f|4\rangle_b|0\rangle$ stretching overtone to occur. Allied to this effort, a new database of water monomer absorption lines was constructed from the best experimental and theoretical data currently available. This UCL08 line list covers the frequency range $750–20\,000\,cm^{-1}$ and is presented in HITRAN file format in this paper's accompanying data. The intensity-weighted average line strengths in UCL08 are within 2.5% of HITRAN08 in the regions $6000–8000\,cm^{-1}$ and $9500–11\,000\,cm^{-1}$ (although there are significant line-by-line differences, especially for weaker lines), but is some 20% stronger for UCL08 in the $8000–9500\,cm^{-1}$ region. Of direct relevance to our search for a water dimer signal, the UCL08 list contains many additional lines in "quieter" spectral regions in between monomer bands, i.e. in regions offering experimental advantages for observing red-shifted dimer bands.

ACPD
10, 23345–23380, 2010

(It may also be worth incorporating the extra lines in radiative budget calculations, cf. Learner et al., 1999, Zhong et al., 2001.) Compared to HITRAN08, the UCL08 line list was found to produce a better fit to the monomer structure (smaller residuals) in broadband cavity ringdown spectra of water vapour in the wavelength region 736–759 nm.

Laboratory measurements were made to attempt to reproduce the absorption feature observed and assigned to water dimers by Pfeilsticker et al. (2003), but no such signal was found in the BBCRDS spectra. Further experiments conducted at high relative humidity and elevated temperatures (up to 85% RH at 312 K) to increase the dimer number density by a further factor of ten also found no signal that could unambiguously be assigned to water dimer absorption when the new UCL08 database was used to fit the water monomer component of BBCRDS spectra. Moreover, if the dimer signal is constrained to have a half width similar to that observed for the dimer's fundamental, first overtone and low combination bands ($\gamma \approx 25\,\mathrm{cm}^{-1}$), water dimer absorptions calculated using dimer line intensities from the available theoretical studies and the Curtiss et al. equilibrium constant were found to be very much greater than the maximum possible dimer signal in the BBCRDS spectra. Since it is unlikely that water dimer line strengths from theory could be wrong by an order of magnitude, this result implies that the HWHM of the high overtone water dimer absorptions must be somewhat greater ($>100\,\mathrm{cm}^{-1}$) than previously observed for dimer bands at longer wavelength. The minimum HWHM inferred for water dimer transitions in the present 750 nm region is consistent with predictions from recent theoretical work that shows dimer bands becoming increasingly broad for higher vibrational overtones due to coupling of the OH_b stretching motion with other internal modes of the molecule (Garden et al., 2008). The BBCRDS measurements described here provide a useful upper limit for further calculations to predict the shape and magnitude of water dimer absorption.

ACPD
10, 23345–23380, 2010

Supplementary material related to this article is available online at: http://www.atmos-chem-phys-discuss.net/10/23345/2010/acpd-10-23345-2010-supplement.zip.

Acknowledgements. This work was conducted as part of the CAVIAR consortium supported by the Natural Environment Research Council. We specifically acknowledge PhD studentships for A.J.L.S. and M.J.B., and grant awards to Cambridge University (NE/D013046/1), Leicester University (NE/D010853/1) and University College London (NE/D013003/1). We thank R. J. Barber for help with including theoretical lines in the UCL08 line list, and colleagues within the CAVIAR consortium (particularly Igor Ptashnik) for helpful discussion.

References

Aldener, M., Brown, S. S., Stark, H., Daniel, J. S., and Ravishankara, A. R.: Near-IR absorption of water vapour: pressure dependence of line strengths and an upper limit for continuum absorption, J. Mol. Spectrosc., 232, 223–230, 2005.

Ball, S. M. and Jones, R. L.: Broad-band cavity ring-down spectroscopy, Chem. Rev., 103, 5239–5262, doi:10.1021/cr020523k, 2003.

Ball, S. M. and Jones, R. L.: Broadband cavity ring-down spectroscopy, in: Cavity Ring-Down Spectroscopy: Techniques and Applications, edited by: Berden, G. and Engeln, R., Blackwell Publishing Ltd, Chichester, West Sussex, UK, 2009.

Barber, R. J., Tennyson, J., Harris, G. J., and Tolchenov, R. N.: A high-accuracy computed water line list, Mon. Not. R. Astron. Soc., 368, 1087–1094, 2006.

Bitter, M., Ball, S. M., Povey, I. M., and Jones, R. L.: A broadband cavity ringdown spectrometer for in-situ measurements of atmospheric trace gases, Atmos. Chem. Phys., 5, 2547–2560, doi:10.5194/acp-5-2547-2005, 2005.

Bouteiller, Y. and Perchard, J. P.: The vibrational spectrum of $(H_2O)_2$: comparison between anharmonic ab intio calculations and neon matrix infrared data between 9000 and 90 cm^{-1}, Chem. Phys., 305, 1–12, 2004.

Casanova, S. E. B., Shine, K. P, Gardiner, T., Coleman, M. and Pegrum, H.: Assessment of the consistency of near-infrared water vapor line intensities using high-spectral-resolution

ACPD
10, 23345–23380, 2010

ground-based Fourier transform measurements of solar radiation, J. Geophys. Res.-Atmos., 111, D11302, doi:10.1029/2005JD006583, 2006.
Cormier, J. G., Hodges, J. T., and Drummond, J. R.: Infrared water vapour continuum absorption at atmospheric temperatures, J. Chem. Phys., 122, 114309, doi:10.1063/1.1862623, 2005.
Coudert, L. H., Wagner, G., Birk, M., Baranov, Y. I., Lafferty, W. J., and Flaud, J.-M.: The $H_2^{16}O$ molecule: line position and line intensity analyses up to the second triad, J. Mol. Spectrosc., 251, 339–357, 2008.
Curtiss, L. A., Frurip, D. J., and Blander, M.: Studies of molecular association in H_2O and D_2O vapors by measurement of thermal conductivity, J. Chem. Phys., 71, 2703–2711, 1979.
Chýlek, P. and Geldart, D. J. W.: Water vapor dimers and atmospheric absorption of electromagnetic radiation, Geophys. Res. Lett., 24(16), 2015–2018, 1997.
Daniel, J. S., Solomon, S., Sanders, R. W., Portmann, R. W., and Miller, D. C.: Implications for water monomer and dimer solar absorption from observations at Boulder, Colorado, J. Geophys. Res.-Atmos., 104, 16785–16791, 1999.
Fellers, R. S., Leforestier, C., Braly, L. B., Brown, M. G., and Saykally, R. J.: Spectroscopic determination of the water pair potential, Science, 284, 945–948, 1999.
Garden, A. L., Halonen, L., and Kjaergaard, H. G.: Calculated band profiles of the OH-stretching transitions in water dimer, J. Phys. Chem. A, 112, 7439–7447, doi:10.1021/jp802001g, 2008.
Goldman, N., Leforestier, C., and Saykally, R. J.: Water dimers in the atmosphere II: results from the VRT(ASP-W)III potential surface, J. Phys. Chem. A, 108, 787–794, doi:10.1021/jp035360y, 2004.
Harvey, A. H. and Lemmon, E. W.: Correlation for the second virial coefficient of water, J. Phys. Chem. Ref. Data, 33, 369–376, doi:10.1063/1.1587731, 2004.
Hill, C. and Jones, R. L.: Absorption of solar radiation by water vapor in clear and cloudy skies: implications for anomalous absorption, J. Geophys. Res.-Atmos., 105, 9421–9428, 2000.
Huisken, F., Kaloudis, M., and Kulcke, A.: Infrared spectroscopy of small size-selected water clusters, J. Chem. Phys., 104, 17–25, 1996.
Jenouvrier, A., Daumont, L., Regalia-Jarlot, L., Tyuterev, V. G., Carleer, M., Vandaele, A. C., Mikhailenko, S., and Fally, S.: Fourier transform measurements of water vapor line parameters in the 4200–6600 cm^{-1} region, J. Quant. Spectrosc. Ra., 105, 326–355, 2007.
Kassi, S., Macko, P., Naumenko, O., and Campargue, A.: The absorption spectrum of wa-

ACPD
10, 23345–23380, 2010

ter near 750 nm by CW-CRDS: contribution to the search of water dimer absorption, Phys. Chem. Chem. Phys., 7, 2460–2467, 2005.
Kuyanov-Prozument, K., Choi, M. Y., and Vilesov, A. F.: Spectrum and infrared intensities of OH-stretching bands of water dimers, J. Chem. Phys., 132, 014304, doi:10.1063/1.3276459, 2010.
Learner, R. C. M., Zhong, W., Haigh, J. D., Belmiloud, D., and Clarke, J.: The contribution of unknown weak water vapour lines to the absorption of solar radiation, Geophys. Res. Lett., 26, 3609–3612, 1999.
Lotter, A.: Field measurements of water continuum and water dimer absorption by active long path differential optical absorption spectroscopy (DOAS), Ph.D. thesis, Department of Physics, University of Heidelberg, 2006.
Low, G. R. and Kjaergaard, H. G.: Calculation of OH-stretching band intensities of the water dimer and trimer, J. Chem. Phys., 110, 9104–9115, 1999.
Mikhailenko, S. N., Albert, K. A. K., Mellau, G., Klee, S., Winnewisser, B. P., Winnewisser, M., and Tyuterev, V. G.: Water vapor absorption line intensities in the 1900–6600 cm^{-1} region, J. Quant. Spectrosc. Ra., 109, 2687–2696, 2008.
Mikhailenko, S. N., Le, W., Kassi, S., and Campargue, A.: Weak water absorption lines around 1.455 and 1.66 µm by CW-CRDS, J. Mol. Spectrosc., 244(2), 170–178, 2007.
Munoz-Caro, C. and Nino, A.: Effect of anharmonicities on the thermodynamic properties of the water dimer, J. Phys. Chem. A, 101, 4128–4135, 1997.
Nizkorodov, S. A., Ziemkiewicz, M., and Nesbitt, D. J.: Overtone spectroscopy of H_2O clusters in the v_{OH}=2 manifold: infrared-ultraviolet vibrationally mediated dissociation studies, J. Chem. Phys., 122, 194316, doi:10.1063/1.1899157, 2005.
Odutola, J. A. and Dyke, T. R.: Partially deuterated water dimers – microwave spectra and structure, J. Chem. Phys., 72, 5062–5070, 1980.
Paul, J. B., Collier, C. P., Saykally, R. J., Scherer, J. J., and O'Keefe, A.: Direct measurement of water cluster concentrations by infrared cavity ringdown laser absorption spectroscopy, J. Phys. Chem. A, 101, 5211–5214, 1997.
Paul, J. B., Provencal, R. A., and Saykally, R. J.: Characterisation of the $(D_2O)_2$ hydrogen-bond-acceptor antisymmetric stretch by IR cavity ringdown laser absorption spectroscopy, J. Phys. Chem. A, 102, 3279–3283, 1998.
Paynter, D. J., Ptashnik, I. V., Shine, K. P., and Smith, K. M.: Pure water vapor continuum measurements between 3100 and 4400 cm^{-1}: evidence for water dimer absorption in near

ACPD
10, 23345–23380, 2010

atmospheric conditions, Geophys. Res. Lett., 34(12), L12808, doi:10.1029/2007GL029259, 2007.
Paynter, D. J.: Measurements and interpretation of the water vapour continuum at near infrared wavelengths, Ph.D. thesis, Department of Meteorology, University of Reading, 2008.
Paynter, D. J., Ptashnik, I. V., Shine, K. P., Smith, K. M., McPheat, R., and Williams, R. G.: Laboratory measurements of the water vapour continuum in the 1200–1800 cm^{-1} region between 293 K and 351 K, J. Geophys. Res.-Atmos., 114, D21301, doi:10.1029/2008JD011355, 2009.
Pfeilsticker, K., Lotter, A., Peters, C., and Bosch, H.: Atmospheric detection of water dimers via near-infrared absorption, Science, 300, 2078–2080, 2003.
Platt, U.: Modern methods of the measurement of atmospheric trace gases, Phys. Chem. Chem. Phys., 1, 5409–5415, 1999.
Ptashnik, I. V., Smith, K. M., Shine, K. P., and Newnham, D. A.: Laboratory measurements of water vapour continuum absorption in spectral region 5000–5600 cm^{-1}: evidence for water dimers, Q. J. Roy. Meteor. Soc., 130, 2391–2408, doi:10.1256/qj.03.178, 2004.
Ptashnik, I. V.: Evidence for the contribution of water dimers to the near-IR water vapour self-continuum, J. Quant. Spectrosc. Ra., 109, 831–852, 2008.
Rothman, L. S., Gordon, I. E., Barbe, A., Benner, D. C., Bernath, P. E., Birk, M., Boudon, V., Brown, L. R., Campargue, A., Champion, J. P., Chance, K., Coudert, L. H., Dana, V., Devi, V. M., Fally, S., Flaud, J. M., Gamache, R. R., Goldman, A., Jacquemart, D., Kleiner, I., Lacome, N., Lafferty, W. J., Mandin, J. Y., Massie, S. T., Mikhailenko, S. N., Miller, C. E., Moazzen-Ahmadi, N., Naumenko, O. V., Nikitin, A. V., Orphal, J., Perevalov, V. I., Perrin, A., Predoi-Cross, A., Rinsland, C. P., Rotger, M., Simeckova, M., Smith, M. A. H., Sung, K., Tashkun, S. A., Tennyson, J., Toth, R. A., Vandaele, A. C., and Vander Auwera, J.: The HITRAN 2008 molecular spectroscopic database, J. Quant. Spectrosc. Ra., 110, 533–572, doi:10.1016/j.jqsrt.2009.02.013, 2009.
Schofield, D. P. and Kjaergaard, H. G.: Calculated OH-stretching and HOH-bending vibrational transitions in the water dimer, Phys. Chem. Chem. Phys., 5, 3100–3105, doi:10.1039/b304952c, 2003.
Schofield, D. P., Lane, J. R., and Kjaergaard, H. G.: Hydrogen bonded OH-stretching vibration in the water dimer, J. Phys. Chem. A, 111, 567–572, doi:10.1021/jp063512u, 2007.
Scribano, Y., Goldman, N., Saykally, R. J., and Leforestier, C.: Water dimers in the atmosphere III: equilibrium constant from a flexible potential, J. Phys. Chem. A, 110, 5411–5419,

ACPD
10, 23345–23380, 2010

doi:10.1021/jp056759k, 2006.
Sierk, B., Solomon, S., Daniel, J. S., Portmann, R. W., Gutman, S. I., Kangford, A. O., Eubank, C. S., Dutton, E. G., and Holub, K. H.: Field measurements of water vapour continuum absorption in the visible and near-infrared, J. Geophys. Res.-Atmos., 109, D08307, doi:10.1029/2003JD003586, 2004.
Suhm, M. A.: How broad are water dimer bands?, Science, 304, 823–823, 2004.
Tennyson, J., Zobov, N. F., Williamson, R., Polyansky, O. L., and Bernath, P. F.: Experimental energy levels of the water molecule, J. Phys. Chem. Ref. Data, 30, 735–831, 2001.
Tolchenov, R. and Tennyson, J.: Water line parameters from refitted spectra constrained by empirical upper state levels: study of the 9500–14 500 cm^{-1} region, J. Quant. Spectrosc. Ra., 109, 559–568, 2008.
Vigasin, A. A.: Water vapor continuous absorption in various mixtures: possible role of weakly bound complexes, J. Quant. Spectrosc. Ra., 64, 25–40, 2000.
Voronin, B. A., Mishina, T. P., Lavrentyeva, N. N., Chesnokova, T. Y., Barber, M. J., and Tennyson, J.: Estimate of the $J' J''$ dependence of water vapour line broadening parameters, J. Quant. Spectrosc. Ra., 111, 2308–2314, doi:10.1016/j.jqsrt.2010.05.015, 2010.
Zhong, W., Haigh, J. D., Belmiloud, D., Schermaul, R., and Tennyson, J.: The impact of new water vapour spectral line parameters on the calculation of atmospheric absorption, Q. J. Roy. Meteor. Soc., 127, 1615–1626 2001.

ACPD
10, 23345–23380, 2010

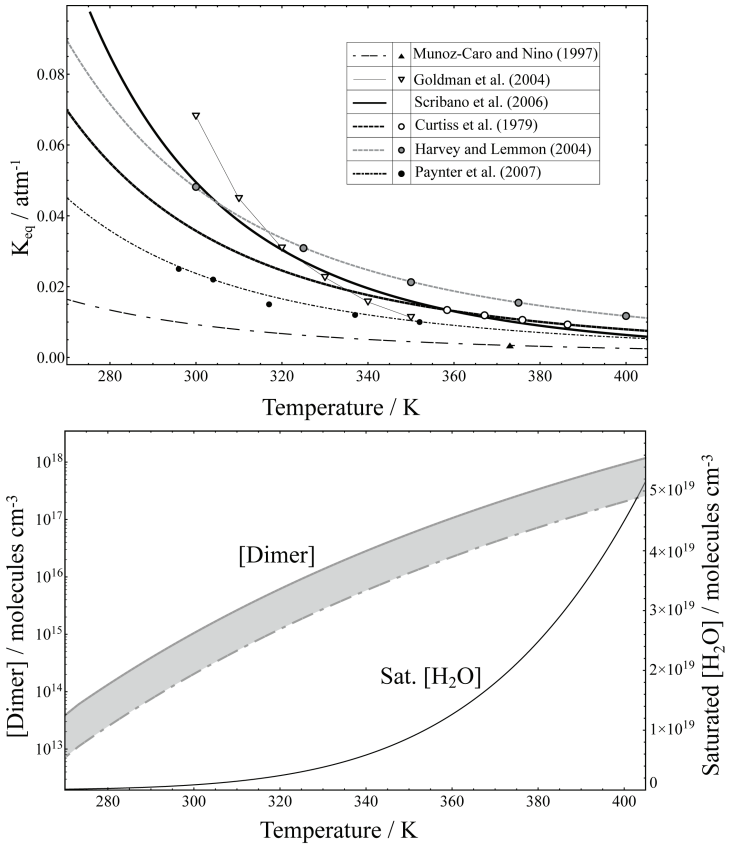

Fig. 1. Upper panel: temperature dependence of the equilibrium constant for formation of the water dimer. Bottom panel: number density of water monomer at saturation as a function of temperature (right axis), and corresponding number density of the dimer (left axis) calculated using the various equilibrium constants above and an assumed relative humidity of 85%.

ACPD
10, 23345–23380, 2010

A upper limit for water dimer absorption

A. J. L. Shillings et al.

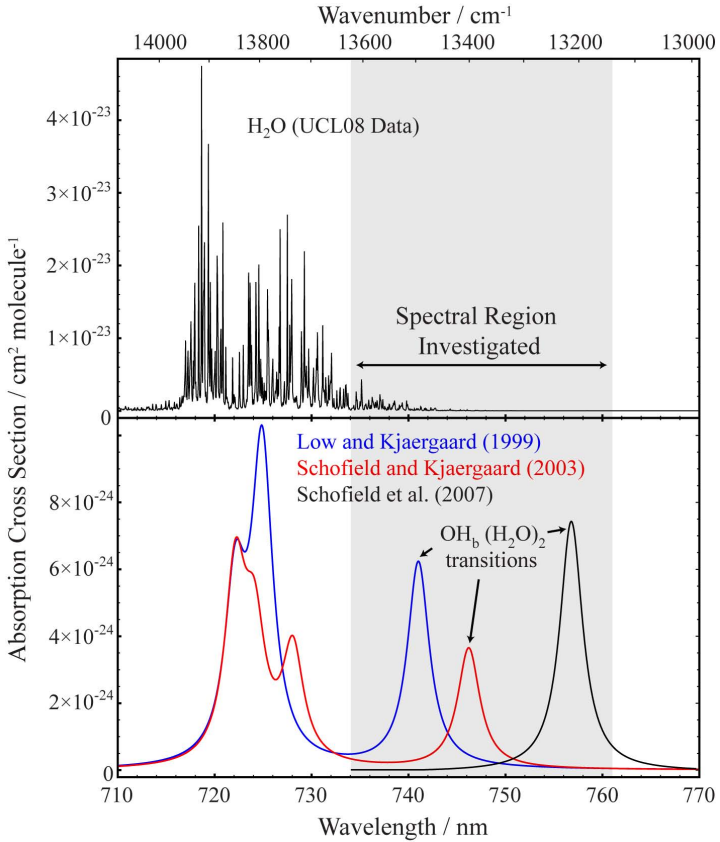

Fig. 2. Water dimer absorption bands at near-infrared wavelengths from theoretical studies for an assumed 25 cm^{-1} HWHM line width (lower panel). For comparison, the upper panel shows high resolution absorption cross sections of the water monomer calculated with the UCL08 line list (air broadened lines). The shaded region indicates the wavelength range of the present BBCRDS measurements.

ACPD
10, 23345–23380, 2010

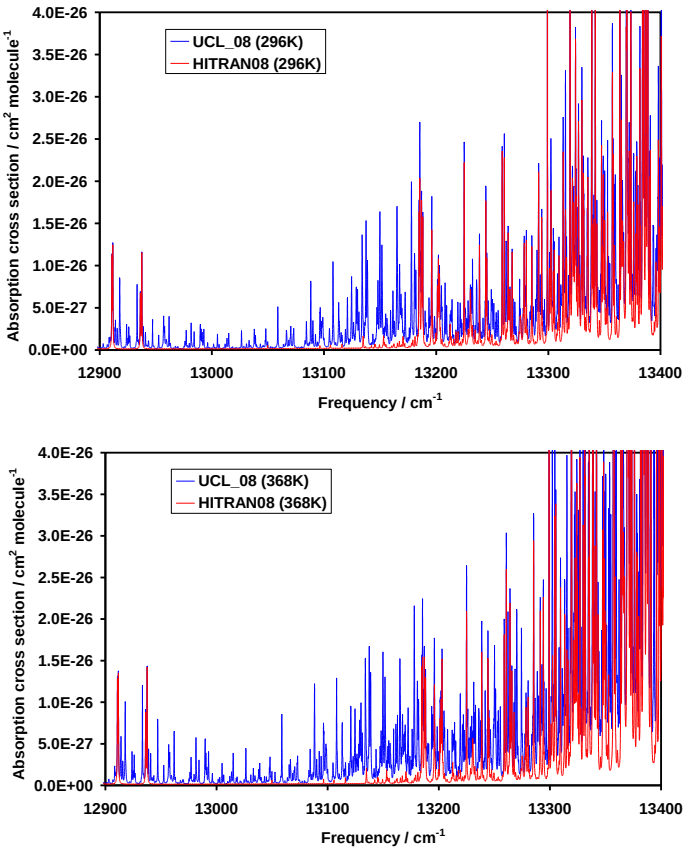

Fig. 3. Comparisons of water monomer absorption cross sections on the low frequency side of the water band around where red-shifted v=4 OH_b dimer vibrations are expected. Cross sections from the HITRAN08 (Rothman et al., 2009; red) and UCL08 line lists (this work; blue) are shown for 296 K and 386 K in the upper and lower panels, respectively.

ACPD
10, 23345–23380, 2010

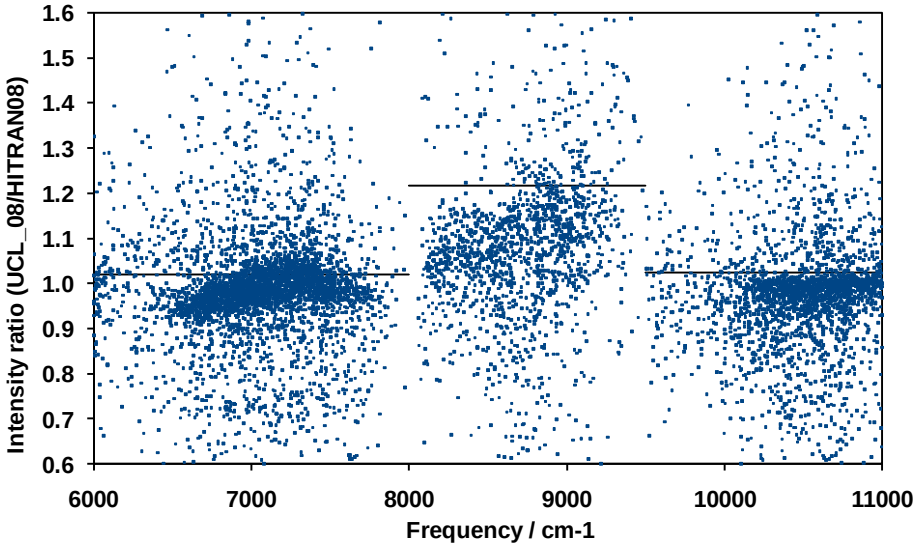

Fig. 4. The ratio of line strengths for water monomer lines common to the HITRAN08 and UCL08 lists. The heavy horizontal lines indicate the intensity-weighted average of the line strength ratios in the spectral regions 6000–8000 cm^{-1} (average=1.0198), 8000–9500 cm^{-1} (1.216) and 9500–11 000 cm^{-1} (1.025).

ACPD
10, 23345–23380, 2010

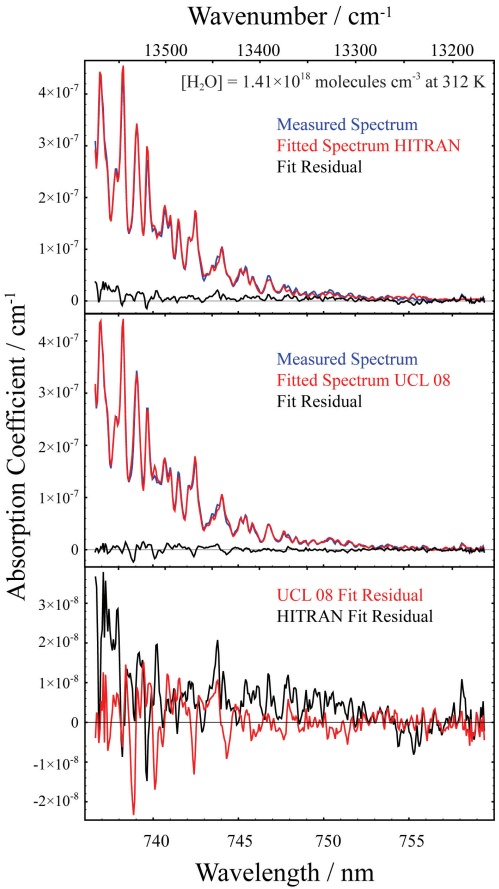

Fig. 5. BBCRDS spectra of water vapour at approx 85% RH at 312 K (blue) fitted with monomer absorption cross sections calculated using the HITRAN08 (red, top panel) and UCL08 line lists (red, middle panel). The residual spectra are shown in black, and are reproduced on an expanded scale in the bottom panel.

ACPD
10, 23345–23380, 2010

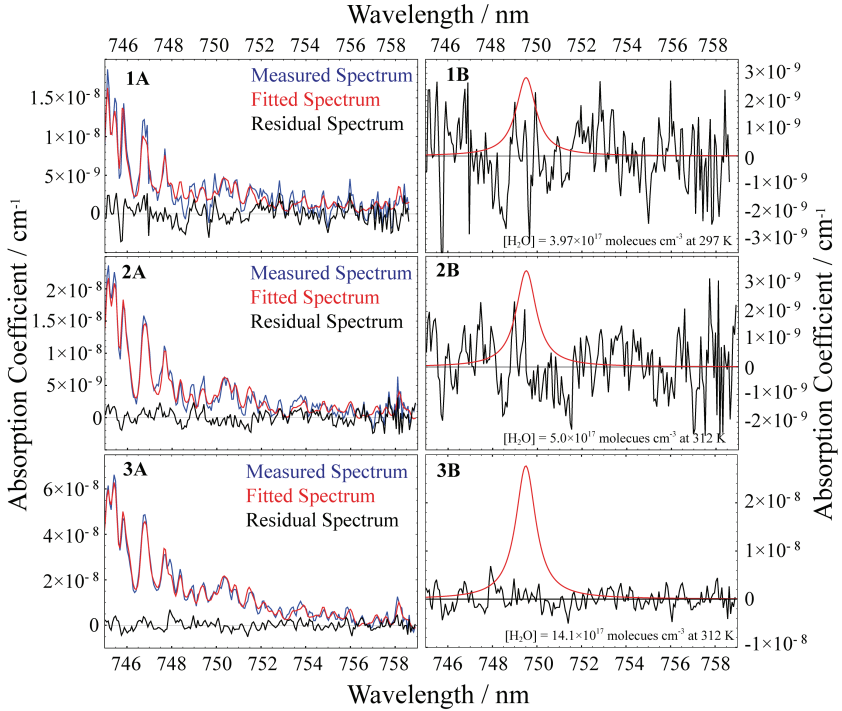

Fig. 6. Panels **(1A)**, **(2A)** and **(3A)**: BBCRDS spectra (blue), corresponding fitted monomer absorption spectra (red; UCL08 line list) and residuals (measurement minus fit; black) for water monomer concentrations of 3.97×10^{17} molecule cm^{-3} at 297 K, 5.0×10^{17} molecule cm^{-3} at 312 K, and 1.41×10^{18} molecule cm^{-3} at 312 K. Panels **(1B)**, **(2B)** and **(3B)** show the corresponding residual spectra again (black), overlaid by a Lorentzian function (red) representing the absorption feature attributed by Pfeilsticker et al. (2003) to the water dimer. This Pfeilsticker absorption feature (PAF) has been appropriately scaled to account for differences in the water monomer concentrations (PAF assumed to scale as $[H_2O]^2$) and the temperature (scaled for $K_{eq}(T)$) between the present studies and the conditions in the Pfeilsticker et al. study. See text for further details.

ACPD
10, 23345–23380, 2010

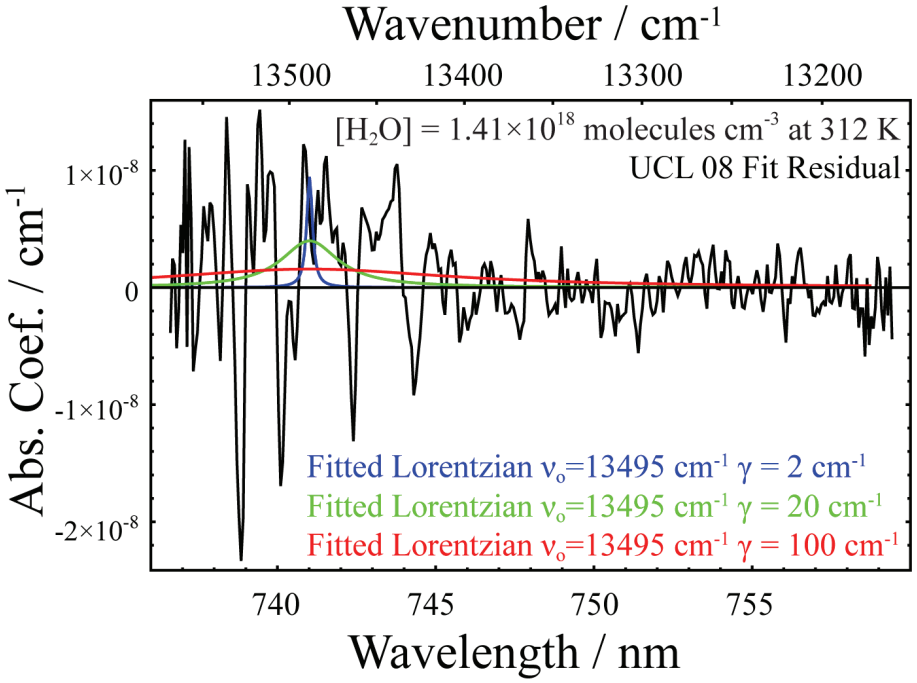

Fig. 7. The residual BBCRDS spectrum from Fig. 6 Panel **(3B)** (black) fitted with Lorentzian functions of various widths (HWHM γ=2, 20 and 100 cm^{-1}; blue, green and red, respectively) centred at the water dimer band frequency predicted by Low and Kjaergaard (1999).

ACPD
10, 23345–23380, 2010

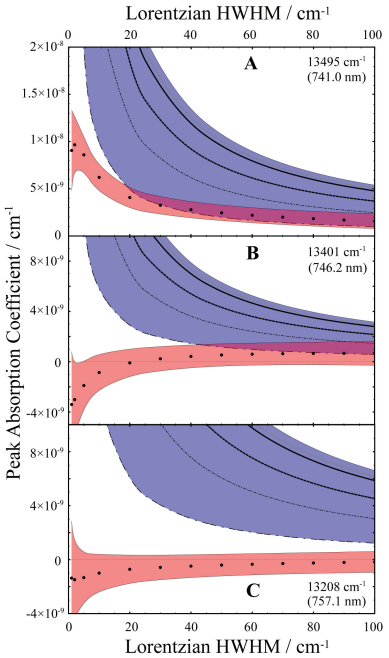

Fig. 8. Upper limits on any dimer signal remaining in the BBCRDS residual spectrum. Panel **(A)**: The peak intensity (black dots) of Lorentzian functions fitted to the BBCRDS residual spectrum shown previously in Fig. 7. The Lorentzian function is centred at 741.0 nm (Low and Kjaergaard, 1999) and has a variable HWHM of γ=1, 2, 5, 10, 20…100 cm^{-1}. The pink shaded area represents the 1σ uncertainty in the fitted Lorentzian function's intensity. The various solid and dashed lines in the blue envelope are HWHM-dependent absorption coefficients for the dimer calculated via Eq. (3) using the various values of K_{eq} from the literature (same line types as Fig. 1) and the Hartree-Fock dimer line strength of Low and Kjaergaard (1999): see the main text. Panels **(B)** and **(C)** are analogous plots generated by fitting the BBCRDS residual spectrum with Lorenztian functions centred at 746.2 nm (Schofield and Kjaergaard, 2003) and 757.1 nm (Schofield et al., 2007).

ACPD
10, 23345–23380, 2010

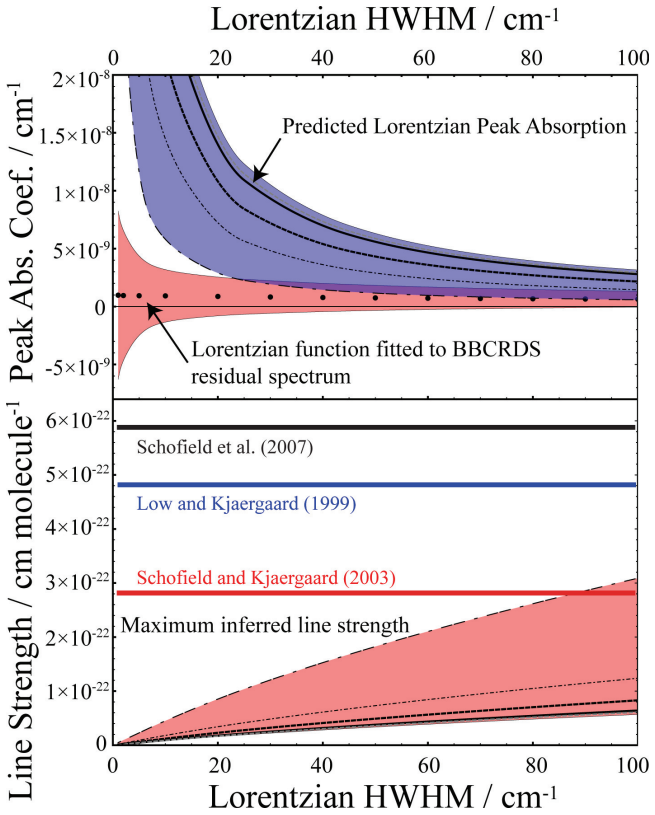

Fig. 9. Upper panel: an analogous plot to Fig. 8 for the average intensity of Lorentzian functions fitted to the BBCRDS residual spectrum in 2 cm^{-1} steps across the full measurement bandwidth. Lower panel: upper limits on the dimer line strengths consistent with the BBCRDS residuals calculated as a function of Lorentzian HWHM (using black dots data from the upper panel) for the different literature values of K_{eq} (lines in pink regions). For comparison, line strengths from the theoretical studies are shown as the heavy horizontal lines.

ACPD
10, 23345–23380, 2010